ADVANCED OPTICAL MATERIALS
www.advopticalmat.de

Femtosecond Direct Laser Writing of Conductive and Electrically Switchable PEDOT:PSS Optical Nanostructures

*Dominik Ludescher, Pavel Ruchka, Leander Siegle, Yanzhe Huang, Philipp Flad, Monika Ubl, Sabine Ludwigs, Mario Hentschel, and Harald Giessen**

Microscale three-dimensional (3D)-printing, with its remarkable precision and ability to create complex structures, has transformed a wide range of applications, from micro-optics and photonics to endoscopy and quantum technologies. In these fields, miniaturization plays a crucial role in unlocking new capabilities. However, despite these advancements, most 3D-printed optical structures have remained static, lacking dynamic behavior and tunability. In this study, a novel approach is presented that combines direct laser writing with the electrically switchable optical properties of the conductive polymer poly(3,4-ethylenedioxythiophene):poly(styrene sulfonate) (PEDOT:PSS). This integration facilitates the creation of dynamic structures directly on 3D-printed objects, marking a significant step toward adaptive optical devices. The fabrication of electrically tunable structures is demonstrated via direct laser writing using PEDOT:PSS on indium tin oxide (ITO)-coated glass substrates, as well as beneath and atop static 3D-printed structures. It is found that electrical conductivity as well as the greyscale behavior of PEDOT:PSS remains intact after direct laser writing. The switching speed, durability, and gradual tunability of the material are explored upon complementary metal-oxide-semiconductor (CMOS)-compatible voltages ranging from −3 to +2 V. In the future, this advancement opens exciting possibilities in adaptive micro-optics, such as switchable apertures printed directly onto micro-optical lenses.

1. Introduction

The fabrication of micro- and nanoscale devices via direct laser writing (DLW) has become increasingly relevant for various applications in optics,[1–4] nanophotonics,[5–7] biotechnology,[8–11] and micro/nanofluidics.[12,13] Introduced in 1997, DLW offers high spatial resolution, fast processing times, material flexibility, and the capability to produce free-form structures.[14] While alternative methods such as inkjet printing and electron beam lithography (EBL) offer specific advantages, the combination of precision and versatility makes DLW uniquely beneficial. The technique typically uses a pulsed femtosecond laser beam (often at $\lambda = 780$ nm) to alter material properties through polymerization or solubility modulation, allowing for the formation of complex structures.

Conventional photoresists utilized for DLW are usually insulating and lack electronic functionality, limiting a wider range of applications. Moreover, even though printed free-form optics are considered to be the future of modern optics,[15] these structures do not have any dynamic character, resulting in static miniaturized devices such as lenses,[2,3] fiber optics,[5–11] or diffractive optics.[4]

In general, there is a twofold interest in advancing the DLW fabrication. First, there is a growing interest in printing conductive structures, essential for applications in electronic circuits,[16,17] sensors,[18,19] and nanophotonics.[20–22] There have been different approaches to incorporate conductive materials into rapid prototyping via DLW, most of them have focused primarily on metal nanoparticles within photosensitive resists, or on photoinitiated reduction of metal ions.[23–25] However, these approaches face challenges, such as slow growth rates, high surface roughness, and in the case of silver nanoparticles susceptibility to oxidation, which limits their applicability and resolution.

Recent efforts have explored alternatives, such as gold nanostructures formed by photo-polymerization of water-based resists or using light-sensitive gold nanoclusters.[26–28] While being promising approaches, these methods still produce structures with high surface roughness and limiting conductivity, still requiring more effective strategies to create conductive and favorably transparent structures that can be seamlessly integrated into

D. Ludescher, P. Ruchka, L. Siegle, P. Flad, M. Ubl, M. Hentschel, H. Giessen
4th Physics Institute and Research Center SCoPE
University of Stuttgart
Pfaffenwaldring 57, 70569 Stuttgart, Germany
E-mail: giessen@pi4.uni-stuttgart.de
Y. Huang, S. Ludwigs
IPOC – Functional Polymers, Institute of Polymer Chemistry
University of Stuttgart
Pfaffenwaldring 55, 70569 Stuttgart, Germany

The ORCID identification number(s) for the author(s) of this article can be found under https://doi.org/10.1002/adom.202403271

DOI: 10.1002/adom.202403271

optical systems. Other approaches, such as blending photopolymers, photoinitiators, and conductive polymers have demonstrated the ability to create conductive structures. However, these methods necessitate the preparation of complex mixtures, adding significant challenges to the fabrication process.[29]

In addition to creating conductive structures, another critical challenge in DLW is introducing dynamic functionality into printed devices. To address both conductivity and dynamic tunability, the conductive polymer poly(3,4-ethylenedioxythiophene):poly(styrene sulfonate) (PEDOT:PSS) is a primary candidate to be a solution for both issues.[30–32] This material not only is conductive but also possesses the intrinsic property of undergoing electrochemically induced refractive index changes enabling dynamic optical control. The material exhibits tunability in the infrared (IR) between a conductive (oxidized) and insulating (reduced) state (for $\lambda > 1.4$ µm). However, already in the visible the active behavior of the material becomes apparent in its electrochromic change of the transmittance. Even though the material behavior in the IR is usually at the center of interest, the tunability in the visible is particularly attractive for hybrid photopolymer systems. The polymer is usually used as a conductive and transparent electrode that replaces indium tin oxide (ITO) in applications such as AR/VR systems,[33–36] light-emitting diodes,[37–39] or bioelectronics.[40–44] Moreover, the material is particularly attractive due to its mechanical, thermal, and oxidative stability.

Despite its promising attributes, previous work expected PEDOT:PSS to be incompatible with direct photolithography due to the lack of chemical orthogonality with photoresists.[45] Previous publications have addressed these limitations by mixing acrylate-based photoresin (IP-L) with the conductive polymer or have structured the PEDOT:PSS using a photolithographic etch mask.[43,47] Even though these generated structures showed conductive properties, yet only static behavior was investigated. We address these limitations by demonstrating that PEDOT:PSS can be directly structured using DLW due to photon-induced solubility modulation retaining both its conductive *and* switchable properties.

Compared to photolithography, inkjet printing, screen printing, and roll-to-roll approaches can provide very high throughput, but are strongly limited techniques in terms of resolution and accuracy.[47–51] These methods are particularly advantageous for large-scale objects but are incapable of generating small feature sizes of down to a few hundred nanometers. Even though EBL can also be used to structure PEDOT:PSS directly, etch mask approaches and direct patterning using electrons are incompatible with photopolymer structures and require increased patterning time especially when mm-sized structures are needed.[52] Additionally, EBL suffers from increased fabrication complexity. Our three-dimensional (3D)-printing approach leverages the strengths of DLW to enable rapid, high-resolution structuring of PEDOT:PSS keeping the fabrication complexity low, and facilitating the fabrication of hybrid, multifunctional devices.

To the best of our knowledge, direct structuring of switchable materials using DLW has not yet been accomplished. We demonstrate direct structuring of the conducting polymer PEDOT:PSS based on a photon-induced solubility modulation and present the integration of this conductive polymer into hybrid DLW-fabricated optical devices. This approach yields hybrid, dynamic structures with high spatial resolution (down to 400 nm), robust conductive properties, and fast, reversible electro-optical switching. The conductivity is measured at ≈1 S cm^{-1} using four-point probe measurements and we present electro-optical functionality operating at telecom wavelengths ($\lambda = 1.55$ µm). Concluding, we present greyscale operation, enabling precise control over the light diffraction intensity.

2. Experimental Results

2.1. Direct Laser Writing of Conducting and Switchable Structures

The fabrication of switchable conducting polymer structures via DLW relies on photon-induced solubility modulation. The polymer PEDOT:PSS exhibits conductive properties and water solubility in its as-cast state, making it suitable for spin-coating and attractive for applications requiring conductive layers such as electrodes. Upon laser irradiation, areas of PEDOT:PSS exposed to the laser light experience a change in water solubility due to radiation-induced crosslinking between polymer chains. It is assumed that heat generated during the laser exposure drives this solubility change, enabling direct patterning of the polymer without restriction to the source of heat input. As a result, direct structuring of the switchable material is achievable via femtosecond laser irradiation or as previously shown via electron beam lithography.[45]

The fabrication protocol is illustrated in **Figure 1a**. Initially, the liquid PEDOT:PSS solution is drop-casted onto a cleaned, oxygen plasma-treatedITO coated glass substrate and spin-coated to form a homogeneous thin film. The ITO layer ensures electrical accessibility. Spin-coating parameters are chosen to produce a film thickness of 90 nm. Repeating the coating process for a second time results in films with ≈180 nm used for the following experiments. Thicker films can be achieved by lowering the spin-coating speed or by increasing the concentration of the conducting polymer in the liquid solution by partial solvent evaporation. Films up to 500 nm thick were successfully switched using our electrochemical approach, providing enhanced device functionality. However, this benefit comes with the trade-off of slower switching times. To balance these two factors, the thickness of 180 nm was chosen as the optimal compromise. The femtosecond laser is focused through the glass substrate onto the polymer film to define the desired patterns by locally altering the water solubility. Subsequent development is achieved by immersing the sample in water for 90 s where unexposed areas dissolve, while irradiated regions remain intact, preserving the initial film thickness.

PEDOT:PSS thus functions as a negative photoresist. Our proposed photolithographic approach directly structures the conducting polymer, in contrast to conventional methods that rely on the generation of etch masks using photoresists. By eliminating this additional step, our fabrication routine minimizes complexity and keeps the process streamlined.

The described method offers significantly reduced fabrication time compared to the initially utilized electron-beam lithography. While these reductions are substantial, mass fabrication remains unfeasible. Achieving true scalability would require photomask exposure with an optimized dose. Nevertheless, the

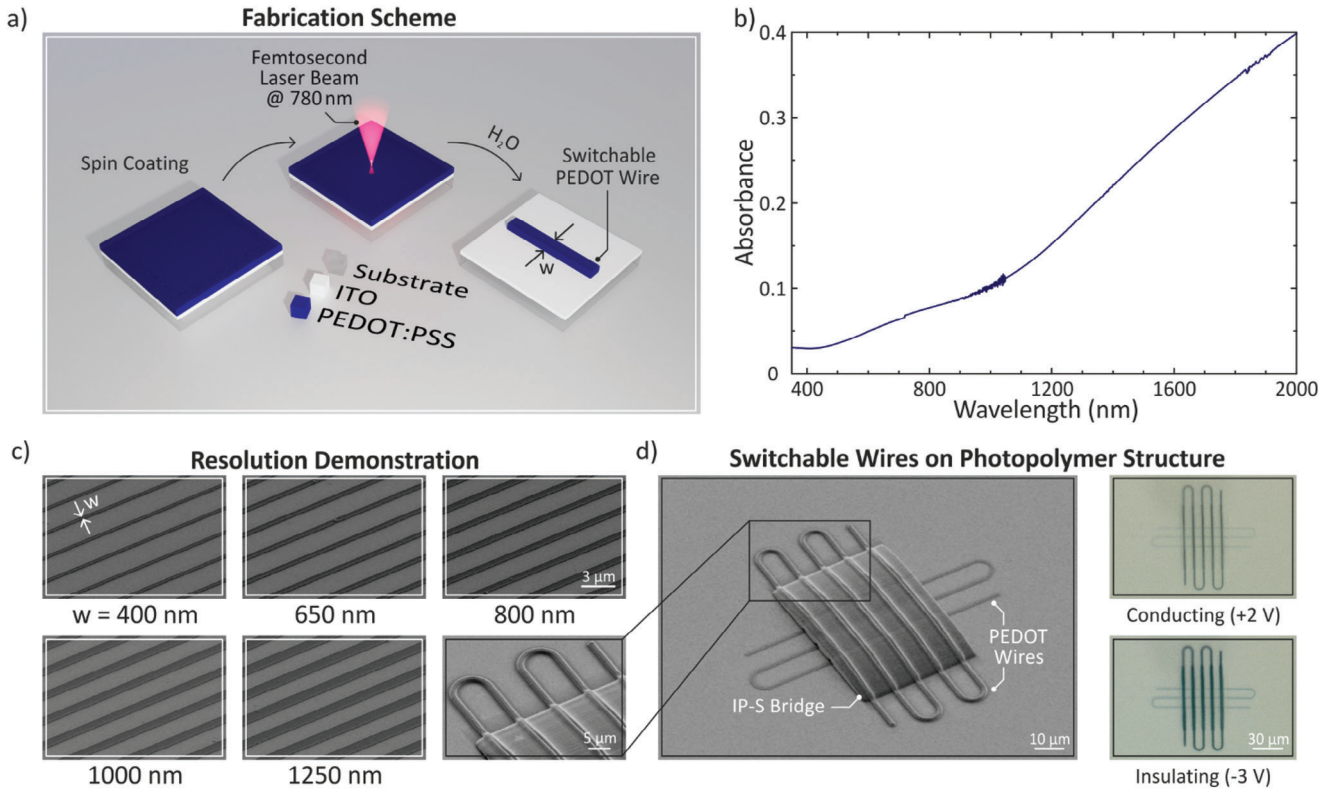

Figure 1. Fabrication of electrically switchable structures via DLW and combination with photopolymer structures. a) Schematic of the fabrication process: A conducting polymer layer (PEDOT:PSS) is spin-coated on an ITO-coated glass substrate (thickness 180 nm). Direct laser writing is performed utilizing a 780 nm femtosecond laser beam, followed by development in water for 90 s to remove unexposed areas. b) Absorbance spectrum for 180 nm PEDOT:PSS from 380 nm to 2 µm, showing increasing absorbance at longer wavelengths measured by UV–vis–NIR spectrophotometry. In (c), the resolution of optical nanostructures is shown. The periodicity of the optical gratings is 3 µm, as the width of the wires ranges from a minimum of 400 nm to 1.25 µm. d) Integration of switchable, conducting polymer wires with conventional photopolymer structures (IP-S). PEDOT:PSS wires are printed on the ITO-coated glass substrate covered by an IP-S bridge. In the next step, conducting polymer wires are fabricated on top of the IP-S bridge. On the left, a zoom-in of the SEM image is shown, on the right, microscope images depict the conducting (+2 V) and insulating state (−3 V).

proposed method greatly simplifies fabrication and lowers costs by eliminating the need for additional evaporation or etching processes.

Figure 1b displays the absorbance spectrum of a 180 nm PEDOT:PSS film, measured from 380 nm to 2 µm using a UV–vis–NIR spectrophotometer. Absorbance increases with wavelength, reaching ≈7.5% at 780 nm. Transmittance spectra of three different film thicknesses are presented in Figure S1 for the metallic and insulating state. Our approach enables high-resolution solubility modulation in the conducting polymer. To establish the resolution limit, nanowires with a periodicity of 3 µm are fabricated, reducing the wire width (w) from 1.25 µm to 400 nm. Below 400 nm, adhesion to the ITO substrate is compromised, thus affecting the required electrical connectivity. The observed limit consequently lies at a width of 400 nm. No residual polymer is observable between the nanowires even with filling factors up to 42%, demonstrating the precision of this fabrication method.

To verify the retention of the electrical properties after patterning, we measured the material conductivity using an established four-point probe (4PP) method (Figure S2). Conductivity measurements on unpatterned films (thickness of 90 and 180 nm) yielded values of ≈0.2 and 0.1 S cm^{-1} respectively, aligning well with previously measured conductivity benchmarks.[45,53] The conductivity increases to ≈1 S cm^{-1} for patterned films with a film thickness of ≈170 nm. To obtain these parameters, a 5 × 0.7 mm^2 patch was patterned using the prescribed fabrication method, and geometric correction factors were applied as in previous studies.[54] Details can be found in the corresponding methods section. The increased conductivity in patterned samples remains unexplained and could be an interesting focus for future research. This behavior can possibly be explained by morphological changes of the conducting polymer upon laser exposure, having a direct impact on direct current (DC) conductivity. Thus, PEDOT:PSS retains its conductive properties post-patterning confirming that DLW is a viable technique for structuring conductive polymer films. A further increase of the DC conductivity is possible using treatment with for example ethylene glycol (EG).[51] Higher conductivities can be achieved by using films with higher crystallinity of PEDOT. However, for the subsequent switching experiments based on the intrinsic redox reaction, altering the electrical properties is not required.

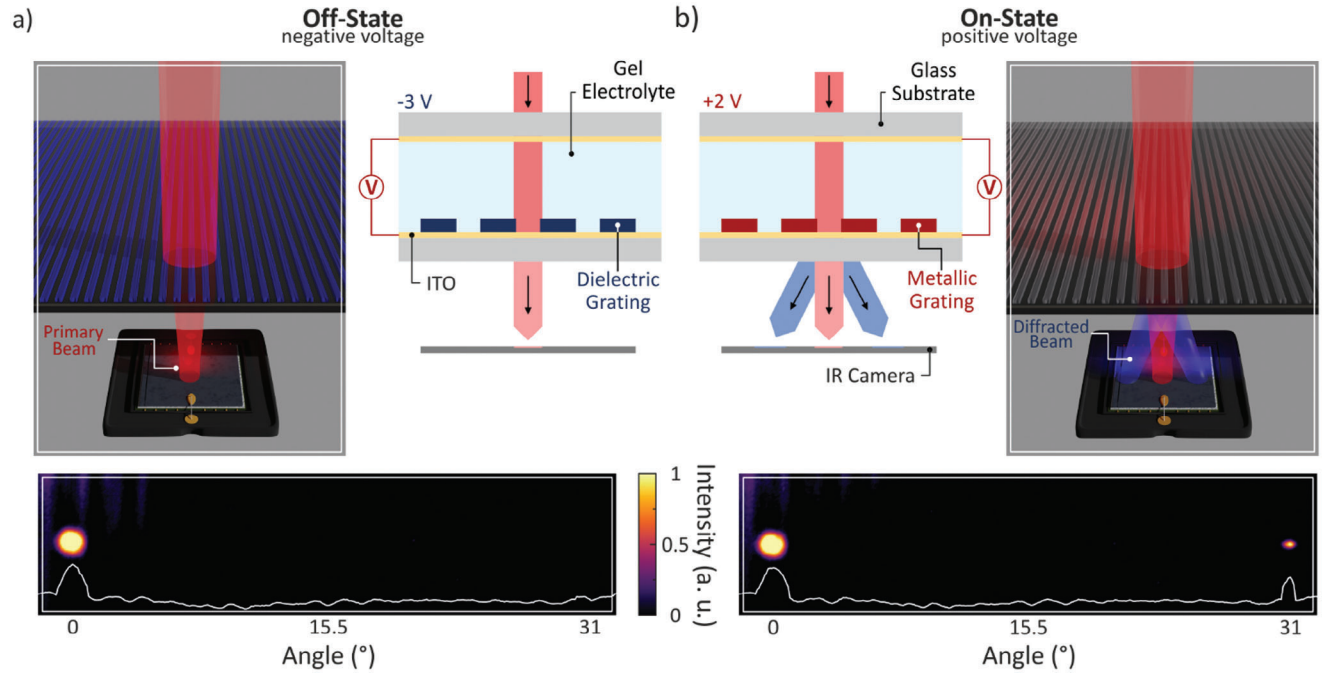

Figure 2. Electrical switching of direct laser written diffraction gratings. Demonstrating the electrical switching between the off-state at a negative voltage (a), and the on-state at a positive voltage (b), by altering the optical properties of the conducting polymer. The center image depicts the electrochemical cell required to drive the redox reaction in the PEDOT:PSS. The cell is formed by two ITO-coated glass substrates enclosing a gel electrolyte. Applying a voltage between the two electrodes enables changes in the optical properties of the conducting polymer. In the on-state, a refractive index difference between the polymer wires and the surrounding electrolyte causes the first diffraction order to appear at an angle of 31°, depicted on the IR camera image on the bottom. The inset provides a cross-section of the image. The zeroth order is attenuated to avoid camera saturation.

2.2. Direct Laser Writing of Switchable PEDOT:PSS Structures on Static 3D Polymers

The miniaturization of optical components is a pivotal focus of optical science. A significant advancement in this domain has been the development of 3D nanofabrication techniques for optical components using DLW with photosensitive polymers. Structures such as lenses and fiber-integrated optics have been successfully fabricated using this technology. We envision that the next crucial progression in this field involves the incorporation of active dynamics into these miniaturized optical components. Consequently, we establish the integration of switchable structures based on the conducting polymer PEDOT:PSS with static photopolymer structures, specifically fabricated from IP-S (Nanoscribe GmbH). Figure 1d illustrates this integration in scanning electron microscopy images of the fabricated hybrid structure. PEDOT:PSS wires are first fabricated on an ITO-coated glass substrate, following the established DLW method. Subsequently, these wires are overlaid with an IP-S bridge, created via DLW using the Nanoscribe Photonic Professional GT. In the concluding fabrication step, the IP-S bridge is coated with PEDOT:PSS through dip-coating and the additional PEDOT:PSS wires on top of the bridge are generated using DLW. Using this 3-step process enables the fabrication of wires underneath the static photopolymer structures as well as wires on top of the IP-S bridge.

The entire PEDOT:PSS structure can be switched repeatedly between the conductive and insulating states, as demonstrated in the images on the right by applying voltages from −3 to +2 V. The conducting polymer is especially interesting due to its intrinsic electrochemically driven metal-to-insulator transition, which allows for the electrical manipulation of the charge carrier density of the material. To control the switching mechanism, a two-electrode electrochemical cell is created based on two ITO-coated glass substrates for electrical access embedding a gel polymer electrolyte in between. A schematic of the cell is presented in the center of **Figure 2**.[55] The gel electrolyte required for the electrochemical redox reaction providing charge neutrality consists of lithium perchlorate ($LiClO_4$) dissolved in polyethylene oxide (PEO) and acetonitrile (ACN) (see methods). Although smaller voltages may already be sufficient, the applied voltages are chosen to ensure that the intrinsic redox reaction is fully driven while remaining in a CMOS-compatible range.

The mixed conductor PEDOT:PSS can reversibly couple ionic and electronic charges, resulting in significant alterations in its doping state, charge carrier density, and, consequently, its optical properties. Applying a negative voltage induces the reduction process of the conducting polymer. The ions from the surrounding electrolyte compensate for the changed charge state resulting in the depletion of hole charges and in the neutral state. This complete dedoping is connected to the loss of delocalized electrons along the polymer backbone. This transition results in a reduced PEDOT:PSS charge carrier density, combined with a modification of the band structure. Changing the applied voltage to a positive voltage, the electrochemical redox reaction leads to an oxidized material state where a high charge current density is present. This observed reaction leads to a significant change

in the dielectric function which can be utilized for tunable and dynamic applications.

In the upper image of Figure 1d, a voltage of +2 V is applied, placing the polymer in its conducting and fully doped state. In this state, the material remains nearly completely transmissive in the visible spectral range. In contrast, applying a voltage of −3 V transitions the polymer into its insulating state. This change in the material state becomes apparent due to a significant color change from transparent to dark blue. Interestingly, the switching is not limited to the material in direct contact with the electrolyte or the ITO but also extends to structures underneath and on top of the insulating IP-S bridge. The IP-S bridge remains barely visible in the two images due to the similar refractive indices of the photoresist and the gel electrolyte. At an incident wavelength of 656 nm, the refractive index of IP-S is $n_{IP\text{-}S}$ = 1.508 compared to $n_{electrolyte}$ = 1.393 for the gel electrolyte.[56] The switching process is fully reversible and operates at CMOS-compatible voltages.

2.3. Electrically Switchable Diffraction Grating for Telecom Wavelengths

This switching mechanism, combined with the fabrication method based on DLW, can now be applied to create an optical diffraction grating, exhibiting functionality at telecom wavelengths (λ = 1550 nm). PEDOT:PSS has its plasma wavelength approximately at 1.4 µm, meaning that for larger wavelengths the material behaves optically metallic. Consequently, at telecom wavelengths, PEDOT:PSS exhibits metallic properties, allowing for strong interactions between the grating and the incident light.

The optical diffraction grating is composed of wires with 1.5 µm width with a periodicity of 3 µm, resulting in a first-order diffraction angle of 31.1°. The electrical tunability of this diffraction grating is demonstrated in Figure 2, where transmitted and first-order diffracted beams are captured using an IR camera.

By adjusting the applied voltage, the diffraction properties can be toggled between on (metallic state) and off (dielectric). In Figure 2a, a voltage of −3 V is applied, placing the material in its dielectric state where the refractive index of the conducting polymer closely matches that of the surrounding PEO-based gel electrolyte. When a voltage of +2 V is applied, the system is switched on as the electrochemical oxidation is triggered, shifting the refractive index of the polymer. This results in a refractive index contrast between the grating material and the electrolyte, leading to diffraction of the incident laser beam and a visible diffraction pattern. The IR camera images at the bottom of Figure 2 depict the purely transmitted beam and the first-order diffracted beam. In the dielectric state, no diffraction is observed while in the metallic state, a first-order diffraction peak becomes apparent at the expected angle of 31.1°. Highlighted by the inset, the profile through the center of the images indicates the same observations. To avoid camera saturation, the zeroth order of the beam is attenuated. The switching of the diffraction properties is repeatable and stable.

Figure 3 illustrates three full switching cycles, with a square wave voltage (15 s per cycle) turning the first diffraction order off (−3 V, white) and on (+2 V, grey) multiple times (Figure 3, bottom).

The counts in the first diffraction order (Figure 3, top) demonstrate rapid switching and a direct correlation between the applied voltage and the intensity of the diffracted beam. The current flow through the electrochemical cell (Figure 3, middle) quickly stabilizes, indicating consistent reduction and oxidization over multiple cycles.

2.4. Switching Speed and Sample Longevity

To gain deeper insights into the switching behavior and electrochemically induced carrier density modulation in DLW-fabricated conducting polymer structures, we investigated the switching speed of these optical devices, displayed in **Figure 4a,b**. Switching off occurs when the voltage is adjusted from +2 V to −3 V while switching the system on is achieved by applying a positive voltage. The laser setup for measuring the switching performance is illustrated in Figure 4c. A helium-neon laser (λ = 632 nm) is focused through an optical chopper wheel operating at 6.4 kHz. The modulated beam is adjusted in size by a telescope to fully illuminate the conducting polymer sample while a potentiostat is used to externally control the redox state of the conducting polymer. The transmitted and modulated signal is then captured by a photodiode and analyzed using a lock-in amplifier.

Examining individual switching events allows us to determine the switching speeds present in the reduction and oxidization of the material.

The fall and rise times, defined as the time span required for a 90% to 10% modulation and vice versa of the transmitted intensity, are highlighted by the grey areas in Figure 4a,b. We observe a rapid, fully reversible switching of the device. The fall time corresponds to a switching speed of τ_{fall} = 0.18 s, and the rise time to τ_{rise} = 0.085 s, resulting in a total duty cycle of 0.265 s or a maximum switching frequency of 3.8 Hz. The slower fall time during reduction indicates a delayed depletion process of the hole charge carriers in the polymer backbone, compared to the faster oxidation process. This aligns with previous observations that the conducting polymer PEDOT:PSS preferentially is present in its oxidized state.[57] Enhancing the switching speed is feasible through various methods as it directly depends on the properties of the conducting polymer thin film and the choice of the electrolyte. For instance, a reduced conducting polymer film thickness directly decreases the switching time. Additionally, switching to a liquid electrolyte could further accelerate the switching due to the increased ion mobility compared to the gel-like electrolyte, although this would add complexity to the electrochemical cell design. In addition, the film treatment and choice of the resistivity of the ITO-coated substrate have a direct impact on the switching speed. Previous studies have found that heat treatment of the PEDOT:PSS film results in increased film stability however leading to the drawback of increased switching times.[55]

We further assessed device durability by performing 250 switching cycles, equivalent to a total switching time of 50 h. Figure 4d presents the transmitted intensity over cycles 1 to 10, 185 to 195 (middle), and 240 to 250 (right), with the corresponding applied voltage displayed below. During each cycle, voltages of −3 and +2 V were applied for 6 min each to allow for full switching of the device. Although the switching time, in the beginning, is significantly shorter than 6 min, this time span for

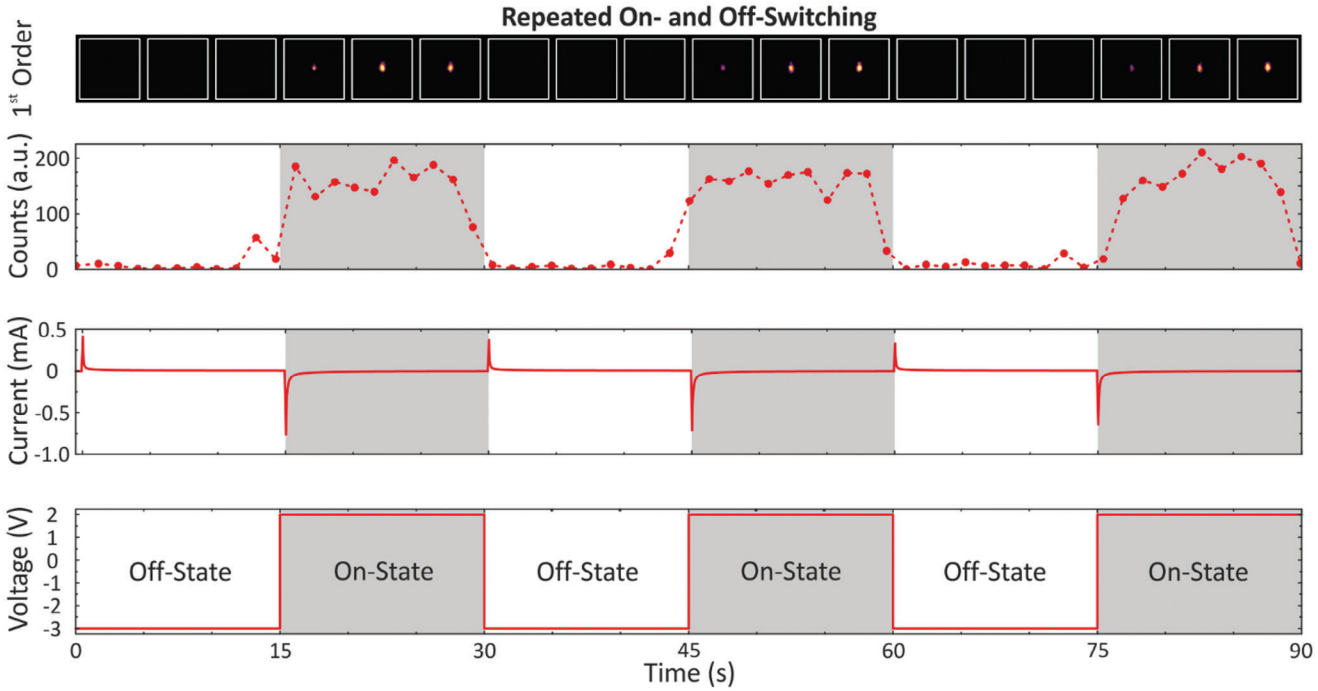

Figure 3. Repeated electrical switching of the diffraction pattern. The diffraction pattern generated by the optical grating can be repeatedly switched on and off by adjusting the applied voltage. (Top) IR camera zoom-in on the first diffraction order, showing the presence or absence of the spot. Underneath the camera images, the counts in the first diffraction order averaged over 2 s are displayed. No counts are detected in the off-state (white), while a clear increase is observed in the on-state (grey). (Middle) Current flow through the electrochemical cell during the switching process, showing a stable switching between the off- and on-state across multiple cycles. (Bottom) The applied voltage is shown, alternating between −3 V (off-state) and +2 V (on-state), each applied for 15 s.

the voltage application was chosen to ensure complete switching even during later cycles, as the switching speed decreases with prolonged operation. Over the time of 50 h, only minor degradation was observed, with a slight decrease in switching contrast (21% modulation reduction). This degradation likely arises from factors such as volume expansion in the conducting polymer, incomplete switching, and gas bubble formation within the ion-gel electrolyte. Nevertheless, the sample maintains homogeneous switching behavior and supports continuous operation of the diffraction grating with no significant decrease in device performance in the solid-state gel polymer setup. More details on the sample durability can be found in Figure S3,S4, and S5, analyzing the transmittance, the current flow through the electrochemical cell, and the switching speed after cycle 1 and cycle 250.

2.5. Greyscale Intensity Tuning

Finally, we examined whether intermediate states between the reduced (−3 V) and oxidized (+2 V) states could be achieved by applying voltages between these endpoints. Successive electrochemical doping would ideally allow for partial electrochemical reactions, leading to gradual changes in the refractive index of the conducting polymer. As the refractive index becomes greyscale-tunable, the diffraction properties directly related to the refractive index difference to the surrounding electrolyte should also exhibit incremental adjustability. This interesting behavior would enable the device not only to toggle between on and off but also to achieve intermediate intensity levels by finely tuning the applied voltage.

In **Figure 5**, this predicted behavior is demonstrated. In Figure 5a, the applied voltage is varied from −1 to +2 V, cycling back to −1 V in steps of 0.5 or 0.25 V. Observing the IR camera images reveals an increase in the intensity of the first diffraction order starting ≈+1.25 V as the material transitions to a more oxidized state, reaching its peak intensity at +1.5 V. This effect enables the control over the amount of light diffracted into the first order. The entire voltage range (−3 to +2 V) was cycled, though only selected IR camera images are shown. The voltages at which the images were captured are marked by the red dots in Figure 5b. The full switching cycles, spanning −3 to +2 V and back, required 500 s. In Figure 5c, a cyclic voltammetry diagram displays the current flow against the applied voltage over four complete cycles to illustrate the electrochemical behavior of the material. In this diagram, the reduction and oxidation points are identifiable, with the cycling direction indicated by the two black dotted arrows. The starting point is at ≈0.5 V cycling toward −3 V indicated by the black point. Upon increasing the potential from −3 to +2 V, the oxidation process is observed. Decreasing the potential to −3 V in the backward scan shows two distinct reduction processes at ≈+0.5 and −1.25 V, which likely involve charge trapping effects, as especially the peak at −1.25 V gains in current during continuous cycling. The behavior is comparable to the electrochemistry of planar PEDOT films in acetonitrile electrolytes.[53,57]

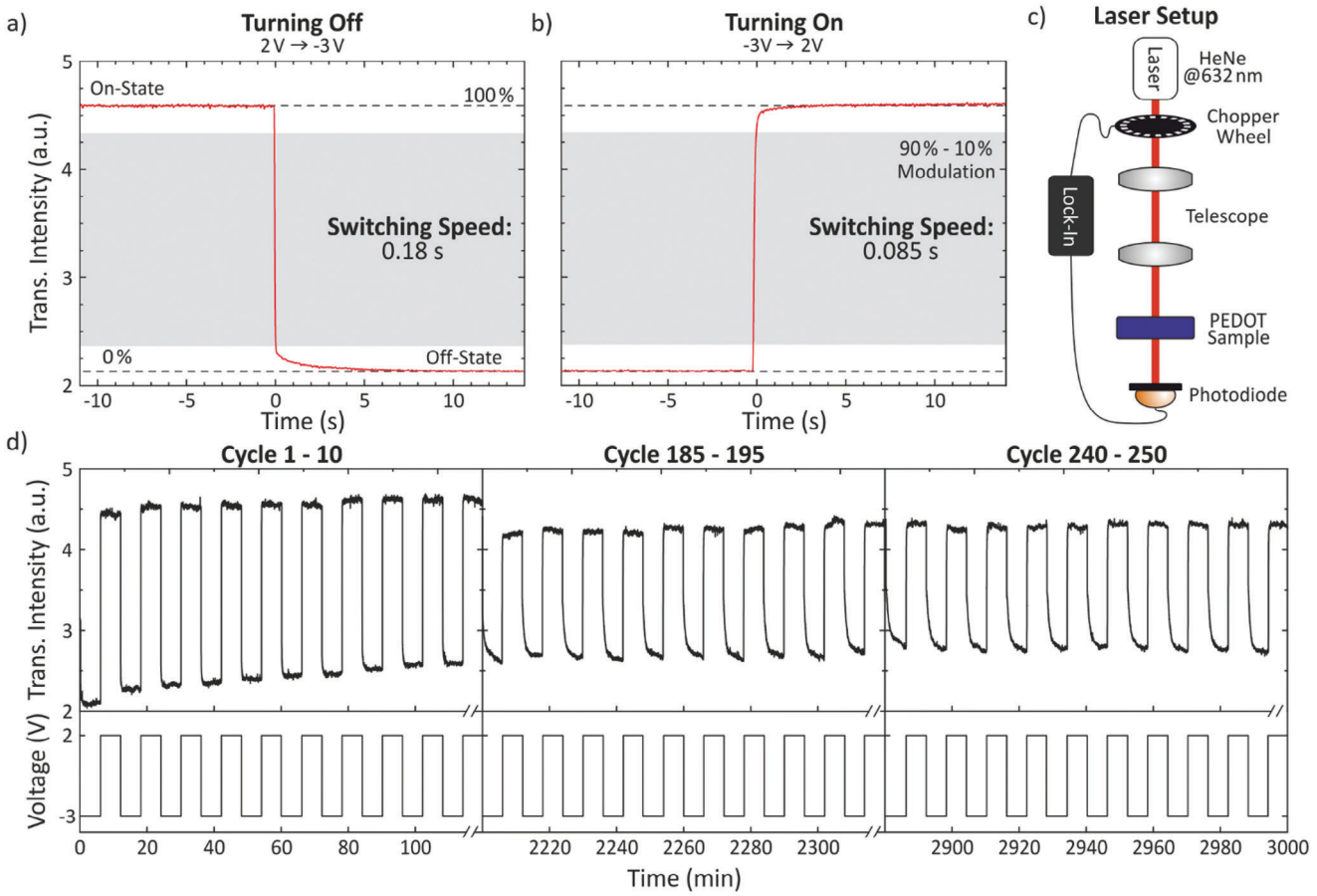

Figure 4. Investigation of the switching speed and sample longevity. The switching speed for turning the diffraction pattern a) off and b) on is presented. The fall and rise curves of the switching process are displayed, with the switching speed defined as the time required to achieve a 90–10% modulation of the transmitted signal. c) The laser setup used to measure the switching speed and the longevity behavior is shown. A 632 nm helium-neon laser, modulated at a frequency of 6.4 kHz by an optical chopper, is focused on the PEDOT:PSS sample. A photodiode detects the transmitted signal, which is analyzed using a lock-in amplifier to assess the switching behavior. d) Longevity is evaluated by examining the transmitted intensity during cycles 1 to 10 (left), 185 to 195 (middle), and 240 to 250 (right). Voltages are applied for 6 min each resulting in a full switching time of 50 h.

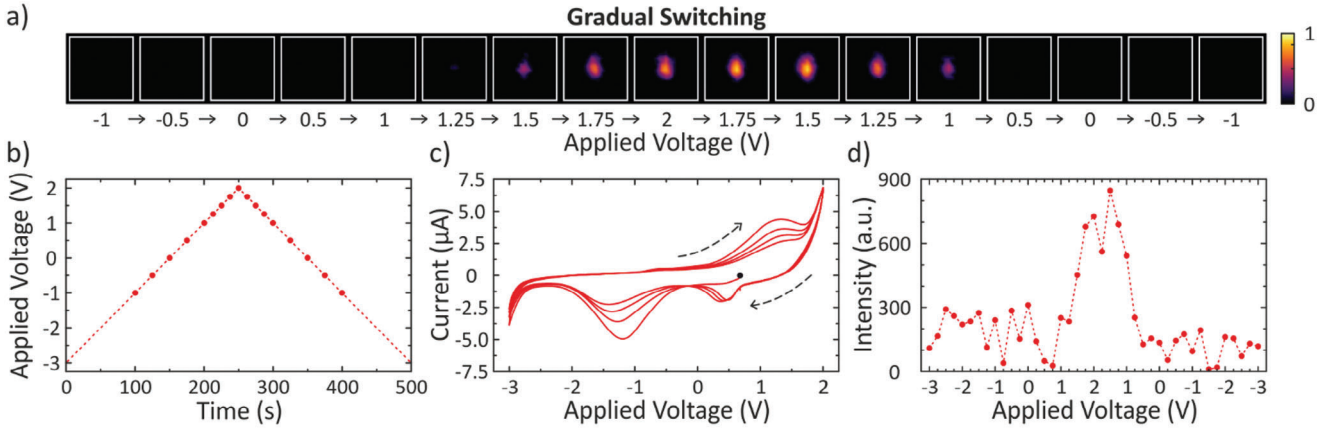

Figure 5. Greyscale intensity tuning. The intensity of the first diffraction order can be gradually adjusted by varying the applied voltage. a) IR camera zoom-in on the first diffraction order, showing a visual increase in intensity as the voltage is changed. b) The applied voltage is changed between −3 V (off-state) and 2 V (on-state) to control the diffraction intensity. The red dots indicate the specific voltages at which the images shown in (a) were captured. c) Cyclic voltammetry diagram for four cycles between −3 and 2 V indicating stable switching behavior. The cycling direction is indicated by the black dotted arrows, the starting point at +0.5 V with the black point. d) The diffracted intensity is plotted as a function of the applied voltage. For voltages <1 V, little to no intensity is detected in the first diffraction order. At higher voltages, a clear increase in the intensity is observed.

In addition, the depicted IR camera images, the measured intensity in the first diffraction order is presented as a function of the applied voltage in Figure 5d. At voltages below +1 V, barely any intensity is detected by the IR camera. However, as the voltage increases, the diffraction intensity rises, corresponding to a growing refractive index contrast between PEDOT:PSS and the surrounding electrolyte. This results in an enhanced diffraction efficiency.

Interestingly, the peak intensity is observed at +1.5 V on the return cycle to −3 V corresponding to the displayed IR camera images. While a decrease in the first-order diffraction intensity would typically be expected, the increased intensity at this point is most likely due to a hysteresis effect seen in the polymer switching behavior. This hysteresis implies that the transition from reduced to the oxidized state does not strictly follow the same route as the other way round, leading to small differences in the refractive index and thus to different diffraction intensities depending on the cycling direction. A similar behavior has been reported for switchable PEDOT:PSS in an earlier publication.[32]

3. Conclusion

In summary, we successfully demonstrated a robust, direct fabrication process for electrically switchable, conducting structures of commercially available polymer PEDOT:PSS, utilizing direct laser writing. The rapid patterning method achieves high spatial resolution and retains the electrical, optical, and switchable properties of PEDOT:PSS, reliably producing polymer nanowires with feature sizes down to 400 nm. In contrast to other fabrication techniques for PEDOT:PSS, this approach allows for the integration of switchable elements with conventional static photopolymer structures, such as IP-S bridges with conducting polymer wires placed both underneath and on top. We consequently establish a new route toward multifunctional miniaturized optical devices.

We further leveraged the technique to fabricate a compact and electrically switchable device for optical beam switching effective at telecom wavelengths. This functionality in combination with greyscale intensity tuning of the diffraction power by accessing intermediate states demonstrates the versatility of PEDOT:PSS for dynamic control of light. Switching speed and long-term stability tests revealed stable and fast switching performance across extensive switching cycles with minimal degradation in modulation contrast.

This work lays the foundation for more complex multifunctional optical systems – such as printed optical lenses with tunable apertures for adjustable brightfield and darkfield imaging, or the integration of switchable materials for the realization of active metasurfaces on optical fibers. Future investigations may explore structuring using continuous wave lasers to further reduce the fabrication time or materials optimized for visible wavelengths, aiming to enhance charge carrier concentrations to enable efficient switching in the visible. Additionally, incorporating a suitable photoinitiator into the switchable material combined with two-photon polymerization facilitates true 3D-printing of stable, switchable structures.

4. Experimental Section

Materials: The samples were prepared using commercially available PEDOT:PSS (Clevios PH 1000, Ossila) with a weight ratio of 1:2.5. Switching experiments were conducted in a home-built electrochemical cell, which encapsulated a gel electrolyte between two ITO-coated 15 × 15 mm^2 glass substrates. The gel electrolyte was composed of polyethylene glycol (PEO, 100 kg mol^{-1}) and lithium perchlorate ($LiClO_4$) in an 8:1 PEO to $LiClO_4$ ratio, dissolved in acetonitrile (ACN) at a concentration of 0.4 g ml^{-1}. All required chemicals for the gel electrolyte were bought from Sigma-Aldrich. No reference electrode was used in this setup. A potentiostat (BioLogic SP-200) was utilized to control the applied voltage. Furthermore, cyclic voltammetry was carried out over four cycles with a voltage range of −3–+2 V at a scan rate of 20 mV s^{-1}.

Thin Film Preparation: The conducting polymer films were generated on ITO-coated glass substrates via spin-coating. The substrates (CEC020T, Präzisions Glas & Optik GmbH) measuring 15 × 15 mm^2 have a thickness of 175 µm. The substrates were cleaned with acetone and isopropyl alcohol (IPA), dried under nitrogen flow, and treated with oxygen plasma for 2 min. The plasma treatment increased the substrate hydrophilicity, enhancing the PEDOT:PSS adhesion and improving the resulting thin film quality.

After substrate cleaning, the conducting polymer PEDOT:PSS was spin-coated. The material was deposited on the sample, spin-coated with 2500 RPM for 5 s, followed by 3000 RPM for 55 s. This procedure was repeated a second time to obtain an increased film thickness. For most of the measurements, the films had a thickness of 180 nm, measured with a contact stylus surface profilometer (Dektak 150 Veeco, Bruker). A single spin-coating cycle yielded a film thickness of ≈90 nm, which was used for the additional conductivity measurement. For the conductivity and absorbance measurements, samples were prepared on glass substrates without the ITO layer.

Absorbance Measurement: The absorbance of a 180 nm thick PEDOT:PSS film was measured from 380 nm to 2 µm using an Agilent CARY 7000 UV–vis–NIR spectrophotometer. The measurements were conducted in double-beam mode with a fixed spectral bandwidth of 2 nm and vertical as well as horizontal apertures of 2°V, ensuring a focused and small beam size on the sample. To maintain accuracy, a data interval of 1 nm and a scan rate of 600 nm min^{-1} were used. PEDOT:PSS was spin-coated on a pre-cleaned and plasma-treated glass substrate resulting in a 180 nm film thickness. The empty substrate itself served as the reference for the measurement.

Four-Point Probe Measurement: The electrical conductivity σ of DLW PEDOT:PSS structures was measured using a four-point probe system (SP4-40045TBS probe head, Signatone, and 2636 system sourcemeter electrometer, Keithley). The conducting polymer was spin-coated as explained before on a pre-cleaned, oxygen plasma-treated glass substrate resulting in films with thicknesses of 90 and 180 nm. A 5 × 0.7 mm^2 square pattern was created to enable the four-point measurement. For comparison, the same measurement was performed on unpatterned 15 × 15 mm^2 PEDOT:PSS to obtain a reference. The conductivity of both patterned and unpatterned samples was calculated using established empirical geometrical correction factors. The conductivity σ is determined by using $\sigma = \rho^{-1}$. The resistivity ρ can be calculated as $\rho = \rho_s \cdot t$, where ρ_s is the sheet resistance and t the film thickness. The sheet resistance ρ_s is determined via $\rho_s = (U/I) \cdot C$, where C is the geometrical correction factor ($C_{film} = 4.3882$, $C_{structured} = 0.7$).[49]

Sample Fabrication by Direct Laser Writing (DLW): The DLW of spin-coated PEDOT:PSS films was performed utilizing a Nanoscribe Photonic Professional GT (Nanoscribe GmbH) with a femtosecond laser at 780 nm with a repetition rate of 80 MHz. All structures were fabricated in oil immersion configuration using a 63x objective. Most of the samples were written with a laser power of 6% (corresponding to 1.3 mW output power after the objective) and a scan speed of 5000 µm s^{-1}. The structures were created by printing 2D lines with 2 µm slicing and a hatching distance of 0.2 µm.

After laser structuring, the sample backside was cleaned with IPA to remove any residual immersion oil. The sample was developed in water for 90 s to remove unexposed areas, leaving only the laser-exposed structures on the ITO-coated glass substrate for switching experiments.

For the bridge structure depicted in Figure 1d, the ITO-coated glass substrate was pre-cleaned and plasma-treated before spin-coating the 180 nm conducting polymer film. The lower conducting polymer wires were fabricated as explained in the main text. After developing the sample in H_2O, the photoresist IP-S was deposited on top of the PEDOT:PSS wires. The bridge was written in oil immersion mode. The bridge has a width of 50 µm, a length of 80 µm, and a total height of 5 µm. Structuring the IP-S used a slicing of 0.1 µm and a hatching of 0.2 µm to ensure smooth curvature of the bridge surface. The sample was developed for 12 min in mrDev-600 (micro-resist technology GmbH) followed by 3 min in IPA.

To obtain the PEDOT:PSS wires on top of the bridge, the sample was dip-coated in the conducting polymer. After structuring the upper PEDOT:PSS wires via DLW, the samples were developed in water for 90 s and dried using nitrogen flow, resulting in fully structured samples.

Electrochemical Switching of the Optical Diffraction Grating at 1550 nm: The fabricated diffraction gratings were analyzed at a telecom wavelength of 1550 nm. A tunable IR laser (Stuttgart Instruments Alpha HP) was adjusted to the desired wavelength. The diffraction pattern was captured using an IR beam profiler (Pyrocam IV, Spiricon). The Beam Gage software was used for image acquisition, and the individually captured images were averaged during post-processing to reduce noise. To prevent saturation of the IR camera, the zeroth order transmitted through the samples was attenuated using a filter.

Switching Speed and Longevity Measurement: The switching speed and sample longevity of the diffraction gratings were evaluated using a helium-neon (HeNe) laser (LHP-151, Melles Griot) at 632.8 nm in an optical chopper setup. The chopper was set to a modulation frequency of 6.4 kHz and the signal was detected using a switchable gain detector (PDA100A2, Thorlabs). The detected signal was analyzed with a lock-in amplifier (MFLI, Zurich Instruments). For switching speed measurements, a time constant of 1 ms was applied, while a time constant of 5 ms was used for longevity tests (Figure S1).

Supporting Information

Supporting Information is available from the Wiley Online Library or from the author.

Acknowledgements

H.G. acknowledges Baden-Wuerttemberg-Stiftung (Opterial), European Research Council (Advanced Grant Complexplas, PoC Grant 3DPrintedOptics), Bundesministerium für Bildung und Forschung (Printoptics, Q.Link.X, QR.X), Deutsche Forschungsgemeinschaft (DFG, German Research Foundation) (SPP1839 Tailored Disorder, 431314977/GRK2642), University of Stuttgart (Terra Incognita), Gips-Schüle-Stiftung, Carl-Zeiss-Stiftung (EndoPrint3D, QPhoton), Vector Stiftung (MINT Innovations), HORIZON EUROPE European Innovation Council (IV-LAB: 101115545), and Ministerium für Wissenschaft, Forschung und Kunst (Innovation Campus Future Mobility: SdManu1, Lab7). M.H. acknowledges the Ministerium für Wissenschaft, Forschung und Kunst Baden-Württemberg (RiSC). Y.H. and S.L. thank the Deutsche Forschungsgemeinschaft (GRK2948/1 Mixed Ionic-Electronic Transport).

Open access funding enabled and organized by Projekt DEAL.

Conflict of Interest

The authors declare no conflict of interest.

Author Contributions

D.L. and P.R. contributed equally to this work. D.L., P.R., and H.G. conceived the project. D.L. and P.R. fabricated the electrically switchable samples, performed the experiments, and carried out the data analysis. L.S., P.F., M.U., and M.H. contributed to the sample fabrication, measurement setup, and experiments. Y.H. and S.L. supported the conductivity measurements. H.G., M.H., and S.L. supervised the project. All authors discussed the results and contributed to the writing of the manuscript.

Data Availability Statement

The data that support the findings of this study are available from the corresponding author upon reasonable request.

Keywords

conductive polymer, direct laser writing, electrically switchable diffraction grating, hybrid switchable photopolymer device, PEDOT:PSS

Received: November 27, 2024
Revised: January 23, 2025
Published online:

[1] D. Gonzalez-Hernandez, S. Varapnickas, A. Bertoncini, C. Liberale, M. Malinauskas, *Adv. Opt. Mater.* **2023**, *11*, 2201701.
[2] T. Gissibl, S. Thiele, A. Herkommer, H. Giessen, *Nat. Photonics* **2016**, *10*, 554.
[3] M. Schmid, S. Thiele, A. Herkommer, H. Giessen, *Opt. Lett.* **2018**, *43*, 5837.
[4] L. Siegle, D. Xie, C. A. Richards, P. v. Braun, H. Giessen, *Opt. Express* **2024**, *32*, 35678.
[5] M. Plidschun, M. Zeisberger, J. Kim, T. Wieduwilt, M. A. Schmidt, *Sci. Rep.* **2022**, *12*, 20920.
[6] L. Bremer, K. Weber, S. Fischbach, S. Thiele, M. Schmidt, A. Kaganskiy, S. Rodt, A. Herkommer, M. Sartison, S. L. Portalupi, P. Michler, H. Giessen, S. Reitzenstein, *APL Photonics* **2020**, *5*, 106101.
[7] P. Ruchka, S. Hammer, M. Rockenhäuser, R. Albrecht, J. Drozella, S. Thiele, H. Giessen, T. Langen, *QST* **2022**, *7*, 045011.
[8] M. H. W. Chin, B. Reid, V. Lachina, S. E. Acton, M. O. Coppens, *Biotechnol. J.* **2024**, *19*, 2300359.
[9] F. Lux, A. Calikoglu, C. Klusmann, M. Hillenbrand, Ç. Ataman, *Appl. Opt.* **2024**, *63*, 2806.
[10] J. Li, S. Thiele, B. C. Quirk, R. W. Kirk, J. W. Verjans, E. Akers, C. A. Bursill, S. J. Nicholls, A. M. Herkommer, H. Giessen, R. A. McLaughlin, *Light: Sci. Appl.* **2020**, *9*, 124.
[11] J. Li, S. Thiele, R. W. Kirk, B. C. Quirk, A. Hoogendoorn, Y. C. Chen, K. Peter, S. J. Nicholls, J. W. Verjans, P. J. Psaltis, C. Bursill, A. M. Herkommer, H. Giessen, R. A. McLaughlin, *Small* **2022**, *18*, 2107032.
[12] O. M. Young, X. Xu, S. Sarker, R. Sochol, *Lab Chip* **2024**, *24*, 2371.
[13] A. T. Alsharhan, O. M. Young, X. Xu, A. J. Stair, R. D. Sochol, *J. Micromech. Microeng.* **2021**, *31*, 044001.
[14] S. Maruo, O. Nakamura, S. Kawata, *Opt. Lett.* **1997**, *22*, 132.
[15] T. Gissibl, S. Thiele, A. Herkommer, H. Giessen, *Nat. Commun.* **2016**, *7*, 11763.
[16] A. Piqué, S. A. Mathews, B. Pratap, R. C. Y. Auyeung, B. J. Karns, S. Lakeou, *Microelectron. Eng.* **2006**, *83*, 2527.
[17] C. Pan, K. Kumar, J. Li, E. J. Markvicka, P. R. Herman, C. Majidi, *Adv. Mater.* **2018**, *30*, 15214095.
[18] Y. Nakajima, K. Obata, M. Machida, A. Hohnholz, J. Koch, O. Suttmann, M. Terakawa, *Opt. Mater. Express* **2017**, *7*, 4203.
[19] M. R. Lee, H. K. Lee, Y. Yang, C. S. L. Koh, C. L. Lay, Y. H. Lee, I. Y. Phang, X. Y. Ling, *ACS Appl. Mater. Interfaces* **2017**, *9*, 39584.
[20] W. Lu, Y. Zhang, M. Zheng, Y. Jia, J. Liu, X. Dong, Z. Zhao, C. Li, Y. Xia, T. Ye, X. Duan, *Opt. Mater. Express* **2013**, *3*, 1660.

[21] A. Ishikawa, T. Tanaka, *J. Laser Micro Nanoeng.* **2012**, *7*, 11.
[22] S. Shukla, E. P. Furlani, X. Vidal, M. T. Swihart, P. N. Prasad, *Adv. Mater.* **2010**, *22*, 3695.
[23] E. H. Waller, S. Dix, J. Gutsche, A. Widera, G. von Freymann, *Micromachines* **2019**, *10*, 827.
[24] M. Focsan, A. M. Craciun, S. Astilean, P. L. Baldeck, *Opt. Mater. Express* **2016**, *6*, 1587.
[25] S. Y. Kang, K. Vora, E. Mazur, *Nanotechnology* **2015**, *26*, 121001.
[26] O. Geladari, M. Eberle, A. Maier, F. Fetzer, T. Chassé, A. J. Meixner, M. Scheele, A. Schnepf, *Small Methods* **2023**, *7*, 2201221.
[27] O. Geladari, P. Haizmann, A. Maier, M. Strienz, M. Eberle, M. Scheele, H. Peisert, A. Schnepf, T. Chassé, K. Braun, A. J. Meixner, *Nanoscale Adv.* **2024**, *6*, 1213.
[28] E. Blasco, J. Müller, P. Müller, V. Trouillet, M. Schön, T. Scherer, C. Barner-Kowollik, M. Wegener, *Adv. Mater.* **2016**, *28*, 3592.
[29] O. Dadras-Toussi, M. Khorrami, L. S. T. Anto Sam Croslee, S. Majd, C. Mohan, M. R. Abidian, *Adv. Mater.* **2022**, *34*, 2200512.
[30] A. J. Heeger, *Chem. Soc. Rev.* **2010**, *39*, 2354.
[31] H. Shirakawa, E. J. Louis, A. G. MacDiarmid, C. H. Chiang, A. J. Heeger, *J. Chem. Soc.* **1977**, *16*, 578.
[32] N. Jeon, J. Noh, C. Jung, J. Rho, *New J. Phys.* **2022**, *24*, 075001.
[33] J. Karst, Y. Lee, M. Floess, M. Ubl, S. Ludwigs, M. Hentschel, H. Giessen, *Nat. Commun.* **2022**, *13*, 7183.
[34] H. S. An, Y. G. Park, K. Kim, Y. S. Nam, M. H. Song, J. U. Park, *Adv. Sci.* **2019**, *6*, 1901603.
[35] S. Chen, M. P. Jonsson, *ACS Photonics* **2023**, *10*, 571.
[36] J. Ratzsch, J. Karst, J. Fu, M. Ubl, T. Pohl, F. Sterl, C. Malacrida, M. Wieland, B. Reineke, T. Zentgraf, S. Ludwigs, M. Hentschel, H. Giessen, *J. Opt.* **2020**, *22*, 124001.
[37] M. M. De Kok, M. Buechel, S. I. E. Vulto, P. Van De Weyer, E. A. Meulenkamp, S. H. P. M. De Winter, A. J. G. Mank, H. J. M. Vorstenbosch, C. H. L. Weijtens, V. Van Elsbergen, *Phys. Status Solidi (A) Appl. Res.* **2004**, *201*, 1342.
[38] G. Heywang, F. Jonas, *Adv. Mater.* **1992**, *4*, 116.
[39] A. Van Dijken, A. Perro, E. A. Meulenkamp, K. Brunner, *Org. Electron.* **2003**, *4*, 131.
[40] D. Lee, J. Song, J. Kim, J. Lee, D. Son, M. Shin, *Gels* **2023**, *9*, 957.
[41] D. Khodagholy, T. Doublet, M. Gurfinkel, P. Quilichini, E. Ismailova, P. Leleux, T. Herve, S. Sanaur, C. Bernard, G. G. Malliaras, *Adv. Mater.* **2011**, *23*, 268 .
[42] S. Conti, *Nat. Rev. Electr. Eng.* **2024**, *1*, 356.
[43] C. Kang, S. Chen, M. Liao, A. Rahmanudin, D. Banerjee, J. Edberg, K. Tybrandt, D. Zhao, M. P. Jonsson, *Npj Flex. Electron* **2024**, *8*, 55.
[44] R. R. M. Serrano, A. Aguzin, E. Mitoudi-Vagourdi, X. Tao, T. E. Naegele, A. T. Jin, N. Lopez-Larrea, M. L. Picchio, M. V. Alban-Paccha, R. J. Minari, D. Mecerreyes, A. Dominguez-Alfaro, G. G. Malliaras, *Biomater* **2024**, *310*, 122624.
[45] S. Doshi, D. Ludescher, J. Karst, M. Floess, J. Carlstrom, B. Li, N. Mintz Hemed, Y. S. Duh, N. A. Melosh, M. Hentschel, M. Brongersma, H. Giessen, *Nanophotonics* **2024**, *13*, 2271.
[46] C. Amruth, A. K. Singh, A. Sharma, D. Corzo, D. Baran, *Adv. Mater. Technol.* **2024**, *9*, 2400290.
[47] S. Ouyang, Y. Xie, D. Wang, D. Zhu, X. Xu, T. Tan, J. DeFranco, H. H. Fong, *J. Polym. Sci., Part B: Polym. Phys.* **2014**, *52*, 1221.
[48] G. B. Tseghai, B. Malengier, K. A. Fante, A. B. Nigusse, L. Van Langenhove, *Sensors* **2020**, *20*, 1742.
[49] A. Singh, M. Katiyar, A. Garg, *RSC Adv.* **2015**, *5*, 78677.
[50] Z. Xiong, C. Liu, *Org. Electron.* **2012**, *13*, 1532.
[51] A. Corletto, J. G. Shapter, *J. Mater. Chem. C* **2021**, *9*, 14161.
[52] J. Karst, M. Floess, M. Ubl, C. Dingler, C. Malacrida, T. Steinle, S. Ludwigs, M. Hentschel, H. Giessen, *Science* **2021**, *374*, 612.
[53] C. Dingler, R. Walter, B. Gompf, S. Ludwigs, *Macromol* **2022**, *55*, 1600.
[54] F. M. Smits, *Bell Labs Techn. J.* **1958**, *37*, 711.
[55] D. de Jong, J. Karst, D. Ludescher, M. Floess, S. Moell, K. Dirnberger, M. Hentschel, S. Ludwigs, P. v. Braun, H. Giessen, *Nanophotonics* **2023**, *12*, 1397.
[56] M. Schmid, D. Ludescher, H. Giessen, *Opt. Mater. Express* **2019**, *9*, 4564 .
[57] M. Wieland, C. Malacrida, Q. Yu, C. Schlewitz, L. Scapinello, A. Penoni, S. Ludwigs, *Flex. Print. Electron.* **2020**, *5*, 014016 .